Impact of heat treatment on the physical properties of sputtered nickel oxide thin films containing molybdenum

M. Sh. Abdel-Wahab[a,b], A. H. Hammad[a,c,*]
[a]*Center of Nanotechnology, King Abdulaziz University, Jeddah 21589, Saudi Arabia*
[b]*Materials Science and Nanotechnology Department, Faculty of Postgraduate Studies for Advanced Sciences, Beni–Suef University, Beni–Suef 62511, Egypt*
[c]*Electron Microscope and Thin Films Department, Physics Research Division, National Research Centre, Dokki, Giza 12622, Egypt*

The effect of annealing the substrate on the structural and optical properties of the nickel oxide thin films containing a fixed ratio of molybdenum was investigated. Energy-dispersive X-ray spectroscopy (EDX) revealed that the Mo ratio is 4.41 wt%. X-ray diffraction (XRD) revealed that the formed films comprise a phase of $NiO_{0.96}$. The average crystallite size, dislocation density, and strain function were calculated. Atomic force microscopy (AFM) was employed to investigate the morphology and surface roughness. With the increase in the substrate temperature from 298 K to 673 K, the optical band gap values varied from 3.72 eV to 3.58 eV.

(Received September 29, 2021; Accepted January 5, 2022)

Keywords: Nickel oxide, Sputtering, Molybdenum, Structure, Optical properties

1. Introduction

Despite the partially filled *3d* orbitals, nickel oxide (NiO) belongs to *3d* transition metal oxides with a NaCl structure, and it is an anti-ferromagnetic insulator with a lattice parameter of 4.173 Å [1,2]. The density of a single crystal of NiO is 6.67 g/cm^3 [2]. The preparation of stoichiometric NiO crystals is difficult in comparison with that of its stoichiometric composition. The NiO crystals are still deficient due to the excess of oxygen [3]. Because the additional oxygen cannot be incorporated into the NaCl structure, Ni^{+2} vacancies are produced, rendering p-type conduction characteristics [4]. Defects such as impurities are typically observed in NiO samples, in addition to the formation of vacancies [3]. The electrical conductivity of NiO significantly varies depending on the preparation process, ranging from 10^{-2} $\Omega^{-1}m^{-1}$ at 500 K to 10^{-10} $\Omega^{-1}m^{-1}$ at 30 K [1]. The valence band (VB) comprises localized nickel *3d* states at ~2 eV from the Fermi stage. X-ray photoelectron spectroscopy (XPS) reveals a small *2p* band, corresponding to oxygen, in the range of 4–8 eV, and a satellite with a potential of up to 8 eV, the latter of which is linked to the core structure of the nickel *3d* states [1]. At a certain photon energy of 2 eV, the refractive index becomes 2.33, and the optical band gab is ~4 eV [5]. Unoccupied nickel *3d*, *4s*, and *4p* states make up the conduction band (CB) [6].

Various physical and chemical techniques can be employed for preparing pure and metal-doped NiO thin films for tuning changes in the surface morphology, optical, and structural properties of the as-prepared NiO films including sol-gel dip-coating [7,8], successive ionic layer adsorption and reaction (SILAR) [9], chemical bath deposition (CBD) [10,11], pulsed laser deposition (PLD) [12–14], spray pyrolysis [15,16], electrodeposition [17–19], and DC sputtering [20–24]. Deposited NiO thin films can be extensively used for various applications, including

* Corresponding author: ahosny2005@gmail.com
https://doi.org/10.15251/JOR.2022.181.1

supercapacitor [25,26], gas sensors [24,27,28], electrochromic application [29,30], buffer layer in the organic solar cell [31,32], and photocatalysis [33–36].

In this study, nickel oxide (NiO_x) thin films doped with Mo by direct current (DC) sputtering are prepared. The prepared films are subsequently annealed at different temperatures under vacuum to investigate the structural changes occurring in the NiO_x lattice. Furthermore, the film morphology, and optical characterization of the samples were investigated to observe the effects of Mo and heat treatment on the NiO_x thin films.

2. Experimental details

A magnetron sputtering system (DC/RF sputtering, Syskey Technologies, Taiwan) was utilized for the deposition of pure and Mo-doped NiO_x thin films at various temperatures of the precleaned glass substrate and silicon wafer. Before deposition, the deposition chamber was evacuated to 1.2 × 10-6 kPa to confirm the absence of contamination in the chamber. The deposited films were prepared using metallic Ni and Mo targets with a DC power set at 200 W for the Ni target and an RF power set at 40 W for the Mo target under fixed argon and oxygen partial pressures of 20 and 10 SCCM, respectively. The deposition time, distance between the target and substrate, and substrate rotation were maintained constant at 30 min, 14 cm, and 15 rpm respectively, during the entire experiment.

The ratio of Mo during deposition and thickness of the deposited films were confirmed by energy-dispersive X-ray spectroscopy (EDX, EMAX model, Japan) and a surface profiler (Bruker, DektakXT, Germany), respectively. X-ray diffraction (Ultima-IV, Rigaku, Japan) was employed to investigate the crystalline phase of the deposited thin films, and the morphology and roughness of the surface-deposited films were determined by atomic force microscopy (AFM, Omicron-VTA-AFM). UV-visible spectrometry (Perkin Elmer Lambda 750, USA) was employed to record the optical transmittance at room temperature.

3. Results and discussion

3.1. Thin-film elemental analysis and thickness measurements

Figure 1 shows the EDS spectrum of the Mo-containing NiO_x thin films containing Mo deposited at 298 K. The ratios of Ni, O, and Mo were 68.26, 27.33, and 4.41 wt%, respectively. Therefore, EDS confirmed that the prepared films are present in the form of oxide, and that Mo is intercalated in the NiO_x thin films as a dopant.

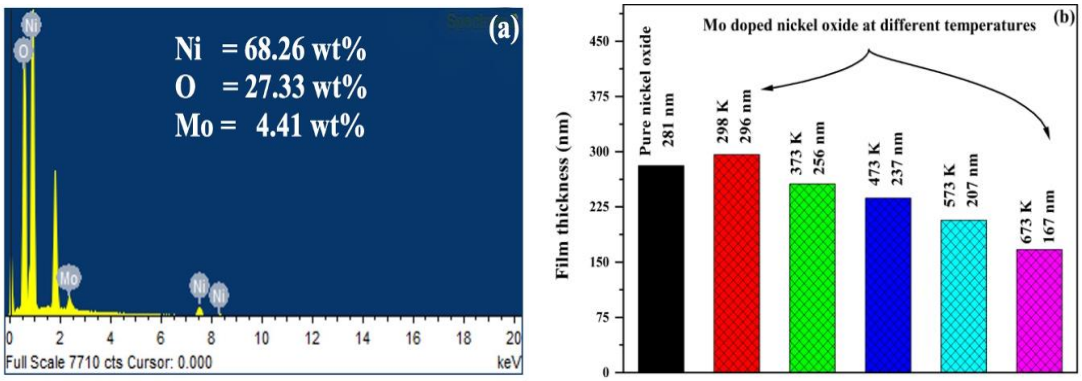

Fig. 1. EDS spectrum of Mo-doped nickel-oxide thin films at 298 K (a), and the dependence of thin film thickness on glass substrate temperatures (b).

The measured thickness of the thin films varied in the range of 167–296 nm depending on the presence of the Mo dopant and glass substrate temperature Figure 1. The film thickness of the pure NiO_x sample was 281 nm at room temperature (298 K), which increased to 296 nm with the introduction of Mo in the NiO_x films. With the increase in the glass substrate temperature from room temperature (298 K) to (373 K), the film thickness reduced to 256 nm, and with the further increase in the temperature, the film thickness further decreased considerably to 167 nm at 673 K. The introduction of Mo in the NiO_x lattice led to increase the film thickness at room temperature due to the higher atomic radius of Mo (1.39 Å) than that of Ni (1.24 Å). With the increase in the glass substrate temperature, the thickness reduced with a value of 167 nm at 673 K, possibly attributed to the higher diffusing rate of Mo (137 KJ/mol) than that of Ni (17.48 KJ/mol); hence, Mo is embedded inside the NiO_x lattice.

3.2. X-ray diffraction investigation

Figure 2 shows the XRD patterns of $NiO_{0.96}$ thin films doped with Mo at different glass substrate temperatures. The pure sample in this study was used as a reference for the other samples discussed in detail by Hammad et al [20]. The prepared exhibited a polycrystalline nature, corresponding to the trigonal crystal system according to the PDF card number (01–078–4383).

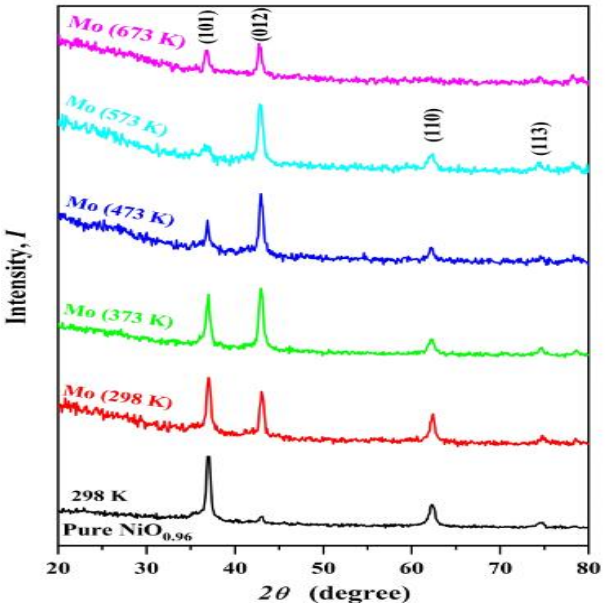

Fig. 2. XRD patterns of sputtered nickel-oxide thin films doped with Mo prepared at different substrate temperatures.

The pure $NiO_{0.96}$ sample exhibited two prominent diffraction peaks characteristic of the (101) and (110) planes, and two weak diffraction peaks corresponding to the (012) and (113) planes, respectively. The (101) plane was the major plane for the reference sample. After the intercalation of Mo into the $NiO_{0.96}$ lattice, significant structural changes occurred. The minor (012) plane grew at the expense of the (101) and (110) planes. With the increase in the substrate temperature from 298 K to 573 K, growth in the diffraction peak intensity and shape broadening was enhanced, while it decreased at a high temperature of 673 K. Moreover, the growth of the (110) and (113) planes was greater than that of pure $NiO_{0.96}$ at 298 K, but the diffraction intensity decreased with the increase in the temperature and diminished at a high temperature of 673 K. Table 1 lists the characteristic planes, diffraction angles, lattice constants, and the unit-cell volume of the sputtered samples.

Table 1. Characteristic planes (hkl), diffraction angle (2θ), interplanar spacing (d-spacing), and unit-cell parameters for $NiO_{0.96}$ thin films containing Mo compared to those in the standard card.

	(101)	(012)	(110)	(113)
Mo (298 K)				
2θ (degree)	36.93	42.98	62.33	74.84
d-spacing (Å)	2.4320	2.1025	1.4885	1.2675
Cell parameters	a = 2.977 Å; c = 7.327 Å; V = 56.2360 $(Å)^3$			
Mo (373 K)				
2θ (degree)	36.90	42.92	62.21	74.62
d-spacing (Å)	2.4340	2.1054	1.4910	1.2707
Cell parameters	a = 2.982 Å; c = 7.283 Å; V = 56.086 $(Å)^3$			
Mo (473 K)				
2θ (degree)	36.90	42.83	62.25	---
d-spacing (Å)	2.4340	2.1099	1.4900	---
Cell parameters	a = 2.980 Å; c = 7.322 Å; V = 56.312 $(Å)^3$			
Mo (573 K)				
2θ (degree)	36.86	42.83	62.33	74.40
d-spacing (Å)	2.4365	2.1097	1.4884	1.2739
Cell parameters	a = 2.976 Å; c = 7.474 Å; V = 57.325 $(Å)^3$			
Mo (673 K)				
2θ (degree)	36.80	42.70	---	---
d-spacing (Å)	2.4417	2.1163	---	---
Cell parameters	a = 2.989 Å; c = 7.349 Å; V = 56.861 $(Å)^3$			
PDF Card No.: 01–078–4383 for $NiO_{0.96}$				
2θ (degree)	36.79	42.74	62.04	74.36
d-spacing (Å)	2.4410	2.1140	1.4950	1.2750
Cell parameters	a = 2.9895 Å; c = 7.3210 Å; V = 56.663 $(Å)^3$			

The average crystallite size (D) of $NiO_{0.96}$ was calculated from the diffraction angle and broadening of the diffraction peaks for the (101) and (012) planes by the use of Scherer's formula as follows [37,38]:

$$D_{(hkl)}=0.89/[\beta_{(hkl)}\cos\theta_{(hkl)}] \quad (1)$$

where λ=0.154056 Å, $\beta_{(hkl)}$ is the diffraction peak broadening of the (hkl) plane, and $\theta_{(hkl)}$ is the diffraction angle of the (hkl) plane. Figure 3 shows the dependence of D for the (101) and (012) planes on the substrate temperature. The crystal size of the (101) plane exhibited the maximum value (~263 Å) at 473 K, related to the high growth of crystals at that temperature. The crystals formed on the (012) plane slowly varied from 298 K to 673 K. However, crystal size exhibited a minimum value (~140 Å) at 573 K. Therefore, the growth of crystals on the (101) plane is more dependent on the substrate temperature than the growth on the (012) plane due to the high growth rate of crystals on the (101) plane in case of the pure $NiO_{0.96}$ sample Figure 2.

The dislocation density (δ) and strain function (ε) on the (101) and (012) planes can be determined from the following equations [21,39,40]:

$$\delta_{(hkl)}=1/D_{(hkl)} \quad (2)$$

$$\varepsilon_{(hkl)}= \beta_{(hkl)}\cos\theta_{(hkl)}/4 \quad (3)$$

Table 2 lists the data calculated for D, δ, and ε. High values for the strain and dislocation density were observed at 573 K for the (101) and (012) planes, although the reference sample of pure $NiO_{0.96}$ exhibited high δ, and ε values for the (012) plane. Hence, the intercalation of Mo in the $NiO_{0.96}$ lattice leads to the decrease in the strain and dislocation density of the crystals grown on the (012) plane.

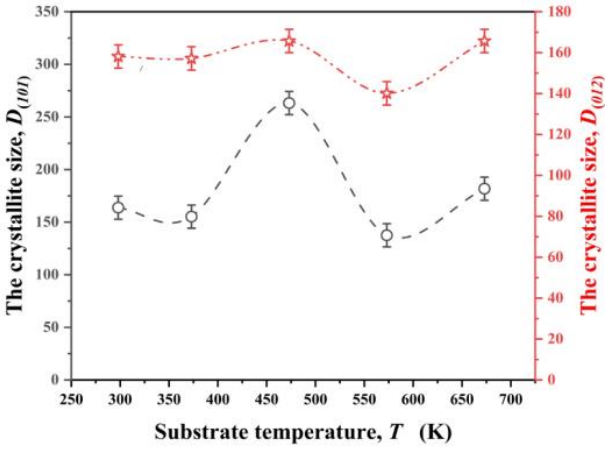

Fig. 3. Dependence of the average crystallite size on the glass substrate temperature.

Table 2. Average crystallite size (D), strain (ε), and dislocation density (δ) of Mo-doped NiO0.96 thin films at different substrate temperatures for (101) and (012) planes.

	(101) plane			(012) plane		
	D±10.86 (Å)	$\delta \times 10^{-5}$ (Å)$^{-2}$	$\varepsilon \times 10^{-3}$	D±5.72 (Å)	$\delta \times 10^{-5}$ (Å)$^{-2}$	$\varepsilon \times 10^{-3}$
Pure $NiO_{0.96}$ (298 K)	200.6	2.48	7.94	121.88	6.73	11.25
Mo (298 K)	163.80	3.73	8.44	158.12	4.00	8.61
Mo (373 K)	155.27	4.15	8.77	157.17	4.05	8.77
Mo (473 K)	263.21	1.44	5.13	165.70	3.64	8.28
Mo (573 K)	137.55	5.28	9.97	140.13	5.10	9.75
Mo (673 K)	181.78	3.03	7.62	165.70	3.64	8.29

3.3. Surface morphology and roughness investigation

Figure 4 shows the morphology and surface roughness of Mo-doped $NiO_{0.96}$ treated at different substrate temperatures. The pure $NiO_{0.96}$ sample was discussed in detail elsewhere [20]. All samples, including the pure one, exhibited spherical grains aggregated on substrate surface. By the addition of Mo to the $NiO_{0.96}$ lattice at room temperature (298 K), the grain size increased from 39.6 nm (pure $NiO_{0.96}$ [20]) to 41.37 nm. Furthermore, the roughness also slightly increased from 1.56 nm to 1.61 nm. With the increase in the substrate temperature, the grain size increased up to 57 nm at 573 K, with a slight decrease to 49.5 nm at 673 K. However, the surface roughness of the sample was stable at 298 and 373 K (~1.6 nm). High roughness for the Mo–$NiO_{0.96}$ films was observed at 473 K, whereas it decreased (1.24 nm) with the further increase in the substrate temperature (Figure 4).

With the increase in the substrate annealing temperature, the $NiO_{0.96}$ grains grew, and owing to the intercalation of Mo in the $NiO_{0.96}$ lattice, the roughness also increased. At a certain temperature (573 K), the grains decomposed, and the roughness decreased, indicating that the formation of homogenous films is started. The film roughness of Mo–$NiO_{0.96}$ treated at 673 K was less than that of pure $NiO_{0.96}$ films due to the dual effect of the Mo dopant and substrate temperature.

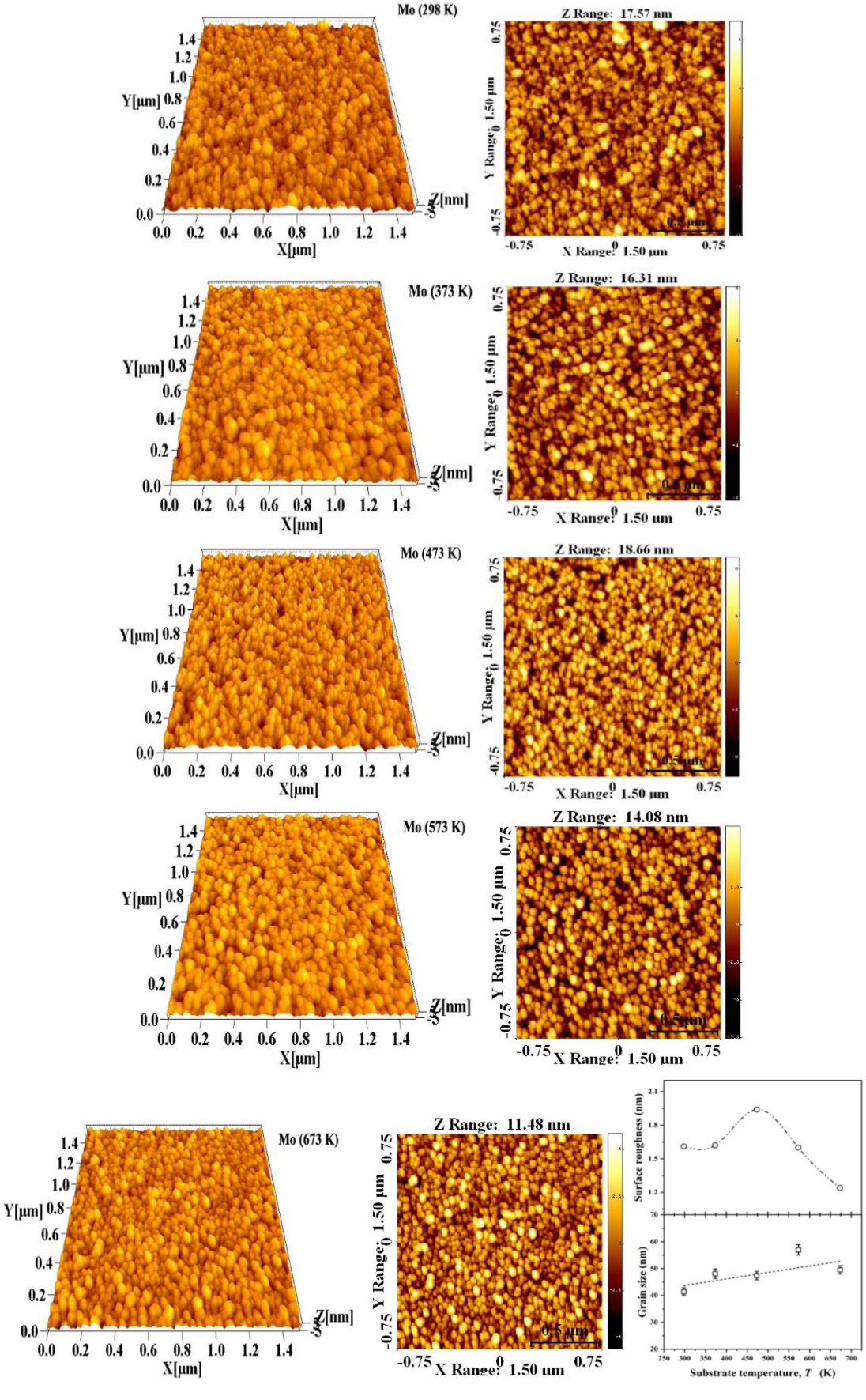
Mo (298 K)
Z Range: 17.57 nm
Mo (373 K)
Z Range: 16.31 nm
Mo (473 K)
Z Range: 18.66 nm
Mo (573 K)
Z Range: 14.08 nm
Mo (673 K)
Z Range: 11.48 nm
Y[μm]
X[μm]
Z[nm]
Y Range: 1.50 μm
X Range: 1.50 μm
0.5 μm
Surface roughness (nm)
Grain size (nm)
Substrate temperature, T (K)

Fig. 4. Film morphology and roughness in two and three dimensions (2D, and 3D), with the dependence of the grain size on the glass substrate temperature.

3.4. Optical properties of Mo–$NiO_{0.96}$ thin films

3.4.1. Optical transmittance

Figure 5 shows the optical transmittance, *T*, of the prepared $NiO_{0.96}$ thin films containing Mo at different substrate temperatures. *T* can be divided into two groups: the first group for films treated at a lower temperature (pure $NiO_{0.96}$, Mo (298 K), and Mo (373 K)), while the second one for films treated at higher temperatures (Mo (473 K), Mo (573 K), and Mo (673 K)).

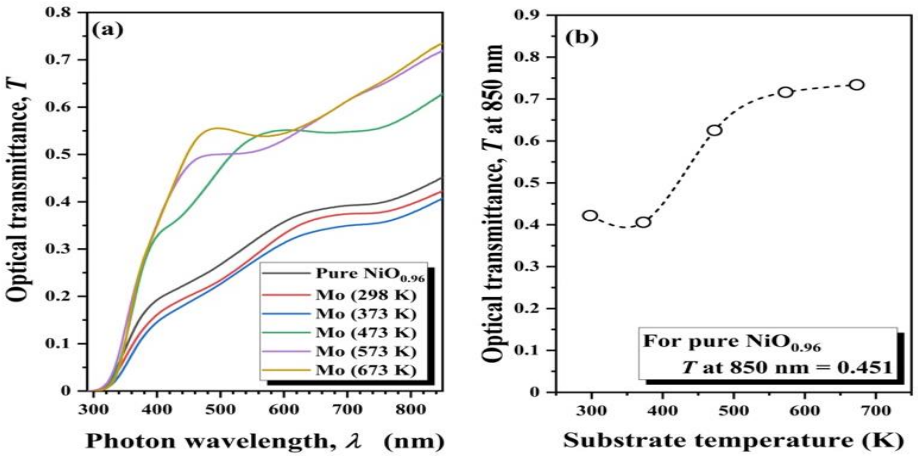

Fig. 5. Optical transmittance and absorption-edge region (a), and the dependence of the optical transmittance on the substrate temperature (b).

With the increase in the temperature to up to 373 K, *T* values of the films healed at low temperature decrease in their intensities to become 0.40 for Mo (373 K). With the increase in the substrate temperature from 473 K up to 673 K, the *T* values increased to become 0.73 for the Mo (673 K) sample. Moreover, the absorption-edge region of the first group was considerably less than that of the second group in length and values. With the increase in the substrate temperature, the absorption edge of each group shifted to long wavelengths. However, the absorption edges of both groups were observed at the cut-off photon wavelength, i.e., $\lambda_{cut\text{-}off}$, of ~296 nm.

3.4.2. Optical band gap and refractive index determination

The current thin films exhibited a polycrystalline nature; therefore, the optical transition of the films is direct transition. The electrons directly move directly between the CB and VB without the absorption or emission of phonons. The optical band gap is determined from the Davis–Mott relation as follows [41]:

$$(\alpha h\upsilon)^2 = G(h\upsilon - E_g) \quad (4)$$

$$\alpha = \ln(1/T)/\text{ Film thickness} \quad (5)$$

where α is the absorption coefficient in cm^{-1}, hυ is the photon energy, G is constant, and Eg is the optical band gap in eV.

Figure 6 shows the determination of the optical transition for the Mo (673 K) sample, as well as the variation in the optical band gap with the substrate temperature. The optical band gap of the pure $NiO_{0.96}$ sample was 3.75 eV [20], which decreased to 3.72 eV after doping with Mo at room temperature. With the increase in the substrate temperature, the optical band gap values decreased to reach 3.58 eV at 673 K. The decrease in the optical band gap value was almost caused by the convergence between the CB and VB, which was affected by the annealing

temperature of the films; this convergence was possibly related to the overlapping of the Mo band structure with the $NiO_{0.96}$ band structure.

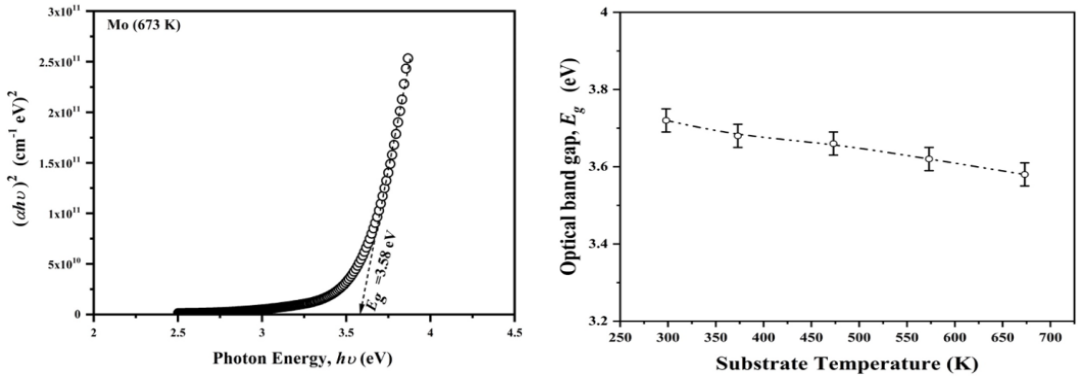

Fig. 6. Optical band gap determination and the dependence of optical transition on the substrate temperature.

The static refractive index, n_o, is correlated to the optical band gap, Eg according to the Moss relation [42], whereas the static, ε_o, and high-frequency dielectric constant, ε_∞, can be estimated from Adachi [20,43]:

$$(n_o)^4 = 95/E_g \quad (6)$$

$$\varepsilon_o = 18.52\text{-}3.08E_g \quad (7)$$

$$\varepsilon_\infty = 11.26\text{-}1.42E_g \quad (8)$$

Table 3 lists the values for $\lambda_{cut\text{-}off}$, E_g, n_o, ε_o, and ε_∞. The optical dispersive parameters are correlated to the optical transition according to the equations (6), (7), and (8). After doping with Mo and after the heat treatment of the substrate, values of these parameters increased. The values of n_o were in agreement with those reported previously [44] for Mo-doped transition-metal oxide such as WO_3.

Table 3. Optical parameters such as the cut-off wavelength, λcut-off, optical band gap, Eg, static refractive index, no, static dielectric constant, ε0, and high-frequency dielectric constant, ε∞.

	Pure $NiO_{0.96}$ [20]	Mo (298 K)	Mo (373 K)	Mo (473 K)	Mo (573 K)	Mo (673 K)
$\lambda_{cut\text{-}off}$ (nm)	290	294	296	298	298	292
E_g (eV)	3.75	3.72	3.68	3.66	3.62	3.58
n_o	2.243	2.248	2.254	2.257	2.263	2.270
ε_o	6.96	7.06	7.18	7.25	7.37	7.50
ε_∞	5.93	5.97	6.03	6.06	6.12	6.18

4. Conclusion

In this study, trigonal $NiO_{0.96}$ thin films containing 4.41 wt% of Mo were prepared by DC/RF sputtering and were investigated as a function of the substrate temperature. The introduction of Mo in the $NiO_{0.96}$ lattice led to the increase in the films thickness from 281 nm for the pure sample to 296 nm for the doped sample. With the increase in the substrate temperature, the film thickness decreased to reach a value of 167 nm at 673 K, indicative of the higher diffusion rate of Mo than that of Ni and the embedding of Mo inside nickel oxide lattice. The average size of

the crystallites exhibited predominant growth on the (101) and (012) planes. Moreover, the doping of $NiO_{0.96}$ with Mo led to the decreased lattice strain and dislocation density with the increase in the substate temperature. Spherical grains of Mo–$NiO_{0.96}$ thin films were observed, and the roughness of such films improved after heating the substrate at 473 K. The optical transmittance of the prepared thin films increased after doping the samples with Mo and with the increase in the substrate temperature. The optical transition was direct, and their values decreased with the increase in the substrate temperature. The band structure of Mo was thought to converge with the band of the $NiO_{0.96}$ lattice, thereby decreasing the optical band gap values. The static refractive index as well as static and high-frequency dielectric constants were correlated to the optical band gap values, which increased with the increase in the substrate temperature.

References

[1] Nobuo. Tsuda, Keiichiro. Nasu, Atsushi. Fujimori, and Kiiti. Siratori, Electronic Conduction in Oxides, Second (Springer, Berlin Heidelberg, 2000); https://doi.org/10.1007/978-3-662-04011-9

[2] D. R. Lide, CRC Handbook of Chemistry and Physics, 80th ed. (CRC Press, Bosa Roca, United States, 2000).

[3] P. Kofstad, Oxidation of Metals 44, 3 (1995); https://doi.org/10.1007/BF01046721

[4] D. Adler and J. Feinleib, Physical Review B 2, 3112 (1970); https://doi.org/10.1103/PhysRevB.2.3112

[5] R. J. Powell and W. E. Spicer, Physical Review B 2, 2182 (1970); https://doi.org/10.1103/PhysRevB.2.2182

[6] H. A. E. Hagelin-Weaver, J. F. Weaver, G. B. Hoflund, and G. N. Salaita, Journal of Electron Spectroscopy and Related Phenomena 134, 139 (2004); https://doi.org/10.1016/j.elspec.2003.10.002

[7] S. Zhao, Y. Shen, P. Zhou, J. Zhang, W. Zhang, X. Chen, D. Wei, P. Fang, and Y. Shen, Ceramics International 44, 753 (2018); https://doi.org/10.1016/j.ceramint.2017.09.243

[8] K. H. Kim, C. Takahashi, Y. Abe, and M. Kawamura, Optik 125, 2899 (2014); https://doi.org/10.1016/j.ijleo.2013.11.074

[9] Y. Akaltun and T. Çayir, Journal of Alloys and Compounds 625, 144 (2015); https://doi.org/10.1016/j.jallcom.2014.10.194

[10] J. H. Yu, S. H. Nam, Y. E. Gil, and J. H. Boo, Applied Surface Science 532, 147441 (2020); https://doi.org/10.1016/j.apsusc.2020.147441

[11] X. H. Xia, J. P. Tu, J. Zhang, X. L. Wang, W. K. Zhang, and H. Huang, Solar Energy Materials and Solar Cells 92, 628 (2008); https://doi.org/10.1016/j.solmat.2008.01.009

[12] M. A. Hameed, O. A. Ali, and S. S. M. Al-Awadi, Optik 206, 164352 (2020); https://doi.org/10.1016/j.ijleo.2020.164352

[13] S. D. Singh, A. Das, R. S. Ajimsha, M. N. Singh, A. Upadhyay, R. Kamparath, C. Mukherjee, P. Misra, S. K. Rai, A. K. Sinha, and T. Ganguli, Materials Science in Semiconductor Processing 66, 186 (2017); https://doi.org/10.1016/j.mssp.2017.04.025

[14] S. Jalili, F. Hajakbari, and A. Hojabri, Journal of Theoretical and Applied Physics 12, 15 (2018); https://doi.org/10.1007/s40094-018-0275-2

[15] B. Gharbi, A. Taabouche, M. Brella, R. Gheriani, Y. Bouachiba, A. Bouabellou, F. Hanini, S. Barouk, H. Serrar, and B. Rahal, Semiconductors 55, 37 (2021); https://doi.org/10.1134/S1063782621010085

[16] H. Hakkoum, T. Tibermacine, N. Sengouga, O. Belahssen, M. Ghougali, A. Benhaya, A. Moumen, and E. Comini, Optical Materials 108, 110434 (2020); https://doi.org/10.1016/j.optmat.2020.110434

[17] L. Zhao, G. Su, W. Liu, L. Cao, J. Wang, Z. Dong, and M. Song, Applied Surface Science 257, 3974 (2011); https://doi.org/10.1016/j.apsusc.2010.11.160

[18] A. Bahramian, M. Eyraud, F. Vacandio, V. Hornebecq, T. Djenizian, and P. Knauth, Journal of Applied Electrochemistry 49, 621 (2019); https://doi.org/10.1007/s10800-019-01305-2

[19] Y. E. Firat, Materials Science in Semiconductor Processing 109, 104958 (2020); https://doi.org/10.1016/j.mssp.2020.104958

[20] A. H. A. H. Hammad, M. S. M. S. Abdel-wahab, S. Vattamkandathil, and A. R. A. R. Ansari, Coatings 9, 615 (2019); https://doi.org/10.3390/coatings9100615

[21] A. H. Hammad, M. S. Abdel-wahab, S. Vattamkandathil, and A. R. Ansari, Physica B: Condensed Matter 568, (2019); https://doi.org/10.1016/j.physb.2019.05.012
[22] K. O. Egbo, C. E. Ekuma, C. P. Liu, and K. M. Yu, Physical Review Materials 4, 104603 (2020); https://doi.org/10.1103/PhysRevMaterials.4.104603
[23] P. Salunkhe, A. V. Muhammed Ali, and D. Kekuda, Materials Research Express 7, 16427 (2020); https://doi.org/10.1088/2053-1591/ab69c5
[24] V. Kampitakis, E. Gagaoudakis, D. Zappa, E. Comini, E. Aperathitis, A. Kostopoulos, G. Kiriakidis, and V. Binas, Materials Science in Semiconductor Processing 115, 105149 (2020); https://doi.org/10.1016/j.mssp.2020.105149
[25] H. K. Jung, S. J. Lee, D. Han, A. R. Hong, H. S. Jang, S. H. Lee, J. H. Mun, H. J. Lee, S. H. Han, D. Yang, and D. H. Kim, Electrochimica Acta 330, 135203 (2020); https://doi.org/10.1016/j.electacta.2019.135203
[26] S. Zhou, S. Wang, S. Zhou, H. Xu, J. Zhao, J. Wang, and Y. Li, Nanoscale 12, 8934 (2020); https://doi.org/10.1039/D0NR01152E
[27] R. Prajesh, V. Goyal, M. Nahid, V. Saini, A. K. Singh, A. K. Sharma, J. Bhargava, and A. Agarwal, Sensors and Actuators, B: Chemical 318, 128166 (2020); https://doi.org/10.1016/j.snb.2020.128166
[28] S. J. Mezher, M. O. Dawood, A. A. Beddai, and M. K. Mejbel, Materials Technology 35, 60 (2020); https://doi.org/10.1080/10667857.2019.1653595
[29] D. Dong, H. Djaoued, G. Vienneau, J. Robichaud, D. Brown, R. Brüning, and Y. Djaoued, Electrochimica Acta 335, 135648 (2020); https://doi.org/10.1016/j.electacta.2020.135648
[30] S. Pereira, A. Gonçalves, N. Correia, J. Pinto, L. Pereira, R. Martins, and E. Fortunato, Solar Energy Materials and Solar Cells 120, 109 (2014); https://doi.org/10.1016/j.solmat.2013.08.024
[31] S. Y. Park, H. R. Kim, Y. J. Kang, D. H. Kim, and J. W. Kang, Solar Energy Materials and Solar Cells 94, 2332 (2010); https://doi.org/10.1016/j.solmat.2010.08.004
[32] K. H. Kim, C. Takahashi, T. Okubo, Y. Abe, and M. Kawamura, Applied Surface Science 258, 7809 (2012); https://doi.org/10.1016/j.apsusc.2012.04.017
[33] A. A. Al-Ghamdi, M. Sh. Abdel-wahab, A. A. Farghali, and P. M. Z. Hasan, Materials Research Bulletin 75, 71 (2016); https://doi.org/10.1016/j.materresbull.2015.11.027
[34] A. Jilani, M. H. D. Othman, M. O. Ansari, R. Kumar, I. U. Khan, M. S. Abdel-wahab, A. Alshahrie, M. A. Barakat, and T. A. Kurniawan, Journal of Materials Science 53, 15034 (2018); https://doi.org/10.1007/s10853-018-2692-7
[35] S. Periyannan, L. Manceriu, N. D. Nguyen, A. Klein, W. Jaegermann, P. Colson, C. Henrist, and R. Cloots, Catalysis Letters 149, 1813 (2019); https://doi.org/10.1007/s10562-019-02781-z
[36] A. F. Kamil, H. I. Abdullah, A. M. Rheima, and S. H. Mohammed, Journal of Ovonic Research 17, 299 (2021)
[37] A. L. Patterson, Physical Review 56, 978 (1939); https://doi.org/10.1103/PhysRev.56.978
[38] G. Gordillo, J. M. Flórez, and L. C. Hernández, Solar Energy Materials and Solar Cells 37, 273 (1995); https://doi.org/10.1016/0927-0248(95)00020-8
[39] G. K. Williamson and R. E. Smallman, Philosophical Magazine 1, 34 (1956); https://doi.org/10.1080/14786435608238074
[40] T. A. Hameed, A. R. Wassel, and I. M. El Radaf, Journal of Alloys and Compounds 805, 1 (2019); https://doi.org/10.1016/j.jallcom.2019.07.041
[41] E. A. Davis and N. F. Mott, Philosophical Magazine 22, 0903 (1970); https://doi.org/10.1080/14786437008221061
[42] T. S. Moss, Physica Status Solidi (b) 131, 415 (1985); https://doi.org/10.1002/pssb.2221310202
[43] S. Adachi, editor , in Properties of Group-IV, III-V and II-VI Semiconductors (John Wiley & Sons, Ltd, Chichester, UK, 2005), pp. 211-281; https://doi.org/10.1002/0470090340.ch10
[44] V. Madhavi, P. J. Kumar, P. Kondaiah, O. M. Hussain, and S. Uthanna, Ionics 20, 1737 (2014); https://doi.org/10.1007/s11581-014-1073-8